processes

MDPI

Article

Research on Process of SCV Flue Gas Carbon Capture Based on LNG Cold Energy

Kun Huang [1,*], Kun Chen [1,*], Cheng Huang [2], Lin Wang [3] and Juan Chen [3]

[1] Petroleum Engineering School, Southwest Petroleum University, Chengdu 610500, China
[2] Institute of Photovoltaic, School of New Energy and Materials, Southwest Petroleum University, Chengdu 610500, China
[3] School of Mechatronic Engineering, Southwest Petroleum University, Chengdu 610500, China
* Correspondence: swpuhk@126.com (K.H.); chenkun9906@126.com (K.C.)

Abstract: Under the guidance of China's goal of achieving carbon neutrality by 2060, the petrochemical industry is increasingly adopting energy-saving and emission-reduction technologies. To realize the low carbon operation of the LNG (liquefied natural gas) receiving terminal, an innovative SCV (submerged combustion vaporizer) flue gas carbon capture system using LNG cold energy was established, and the system also combined with an ORC (organic Rankine cycle). HYSYS software was used to simulate the process of the SCV flue gas carbon capture system and the LNG regasification system. The simulation results showed that the proposed system has low carbon emission and low energy consumption performance. Moreover, the sensitivity analysis of the evaporation pressure of working fluids, CO_2 capture pressure, and CO_2 capture temperature was carried out. The key parameters were optimized by HYSYS software to achieve the optimal operation cost of the system. When the evaporation pressure of working fluids, CO_2 capture pressure, and CO_2 capture temperature were set as 1300 kPa, 750 kPa, and 143.15 K, respectively, the optimized system resulted in an exergy efficiency of 13.63%, an LNG cold exergy utilization rate of 77.49%, a CO_2 capture rate of 94.9%, and a CO_2 capture capacity of 6620.4 kg/h.

Keywords: LNG cold energy; SCV; carbon capture; exergy analysis; parametric analysis

Citation: Huang, K.; Chen, K.; Huang, C.; Wang, L.; Chen, J. Research on Process of SCV Flue Gas Carbon Capture Based on LNG Cold Energy. *Processes* **2022**, *10*, 2546. https://doi.org/10.3390/pr10122546

Academic Editor: Farooq Sher

Received: 12 September 2022
Accepted: 22 November 2022
Published: 30 November 2022

1. Introduction

The "30–60" dual-carbon goal is China's major strategy since Chinese President Xi's announcement to reach peak carbon emissions by 2030 and achieve carbon neutrality by 2060 came out in September 2020. At present, the focus of realizing the dual-carbon goal involves the transformation of the energy structure and the low carbonization of fossil energy. When compared with coal and petroleum, natural gas has clean and low-carbon characteristics, so it plays an irreplaceable role in the process of energy structure transformation and carbon neutrality.

LNG is the main form of international natural gas trading. A standard vessel (125,000 m^3) of LNG emits 220~300 thousand tons of CO_2 equivalent from production to final usage, of which storage and regasification stages account for 0–3% [1]. The LNG receiving terminal can emit about 100 thousand tons of carbon annually [2]. In 2020, direct carbon emissions from SCV at an LNG receiving terminal reached 56 thousand tons. SCV uses the heat generated by the combustion of natural gas to gasify LNG [3,4]. In June 2019, Royal Dutch Shell announced that it had reached the world's first carbon-neutral LNG trade with Tokyo Gas Co., Ltd. and South Korea's GS Energy. As of September 2021, 24 ships running on carbon-neutral LNG have been traded globally [5]. Therefore, it is crucial to capture the carbon of SCV flue gases to achieve low-carbon operation to be carbon-neutral in the LNG receiving terminal. The CC (carbon capture) technologies include the chemical adsorption method, the physical absorption method, the membrane separation method, and the low-temperature separation method, etc. [6,7]. The cryogenic separation method

uses the difference in bubble & dew points of each component in the flue gas, allowing CO_2 to be condensed from the gas phase and transferred to the liquid phase or solid phase by compressing and cooling flue gas several times, to achieve CC. The disadvantage of the cryogenic separation method is that the conventional refrigeration process causes extensive energy consumption. However, at the LNG receiving terminal, the LNG cold energy can be used for the CCC (cryogenic carbon capture) process [8,9].

Domestic and foreign scholars have done a lot of research on using LNG cold energy for CC. Depending on the variance of composition and the CO_2 concentration of the flue gas, the temperature and pressure of the CC vary. For the pure CO_2 flue gas, the conditions of flue gas CC are that the pressure and temperature are below the triple point of CO_2. Shi [10] established a three-stage system for LNG cold energy utilization, including air separation, CO_2 liquefaction, and cold energy power generation. The CO_2 liquefaction rate of the system was 0.223 kg/kg LNG.

For the flue gas with simple composition and high CO_2 concentration, in the process of flue gas CC, the flue gas will be dehydrated and dried, and its carbon capture pressure or temperature becomes higher than the CO_2 triple point. Huang [11] proposed a transcritical RC (Rankine cycle) waste heat power generation and CO_2 liquefaction process, with CO_2 as the working fluid. The exergy efficiency and CO_2 liquefaction rate of the system were 36.33% and 0.273 kg/kg LNG, respectively. On this basis, Wang [12] improved the process. After the flue gas released heat in the RC, it was separated, compressed, and condensed in two stages, and finally exchanged heat with the RC working fluid and LNG to achieve CO_2 liquefaction. The system performance has improved. Xiong [13] and Gomez [14] proposed a zero-carbon emission gas-fired power generation system using LNG cold energy, which combined the RC and BC (Brayton cycle). Liu [15] proposed an innovative CCHP (combined cooling heating and power) system based on the LNG cold energy and the ORC + BC + gas turbine, which realized energy cascade utilization and flue gas CC. The exergy efficiency and CO_2 capture capacity of the system were 62.29% and 79.2 kg/h, respectively. Yu [16] proposed a method to use LNG cold energy to reduce CC energy consumption, which combined the ORC. The system exergy efficiency and CO_2 capture capacity could reach 70% and 15 t/h, respectively. In terms of the Allam cycle using LNG as fuel, Liang [17] proposed a near-zero carbon emission solid oxide fuel cell (SOFC) system based on LNG cold energy and the ORC + RC process. The exergy efficiency and CO_2 capture capacity of the system were 53.07% and 5219.21 t/a, respectively. Ouyang [18] proposed a new LNG cold energy utilization system that combined the ORC and carbon capture cycle. After the optimization of the system process parameters and the circulation of working fluids by genetic algorithm, the system exergy efficiency and CO_2 liquefaction rate were 47.2% and 0.78 t/t LNG, respectively.

For flue gas with multi-component and low CO_2 concentration, the temperature and pressure of flue gas carbon capture are much higher than the triple point of CO_2. Xu [19] and Rifka [20] proposed utilizing LNG cold energy to capture CO_2 in the flue gas. After the flue gas was first compressed and dried, the flue gas was cooled by the LNG cold energy to obtain solid-phase or liquid-phase CO_2. The decarbonized flue gas was discharged to the atmosphere after expansion. Liu [21] proposed a CCHP system based on LNG cold energy and flue gas waste heat combined with CO_2 capture. After the multi-objective optimization of the system, the exergy efficiency and CO_2 capture capacity were 41.38% and 7.9236 t/h, respectively. Zhao [22] proposed a CC system based on the LNG cold energy and industrial flue gas, which also combined the horizontal two-stage ORC. The exergy efficiency and CO_2 liquefaction rate of the system were 57% and 0.75 kg/kg LNG, respectively. Some studies have also combined CCC technology with chemical adsorption [23,24] and membrane separation [25,26] to increase the concentration of CO_2 in the flue gas entering the CCC process.

In this paper, a carbon capture system for SCV flue gas using LNG cold energy is proposed. The system includes an ORC power generation subsystem that uses LNG and SCV flue gas as cold and heat sources. The thermodynamic mathematical model and carbon

emissions mathematical model of the system were established, and the thermodynamic parameters of the system were calculated. The sensitivity analysis of some key process parameters was carried out, and Aspen HYSYS was used to optimize the parameters.

2. System Description

This paper builds an SCV flue gas carbon capture process using LNG cold energy, defined as System A, which consists of the SCV flue gas CC subsystem, an ORC subsystem, an exhausted gas direct expansion cycle (DEC) subsystem, and an LNG regasification subsystem. The HYSYS simulation model of System A is depicted in Figure 1, and the HYSYS simulation model of the conventional LNG regasification system, define as System B, is shown in Figure 2.

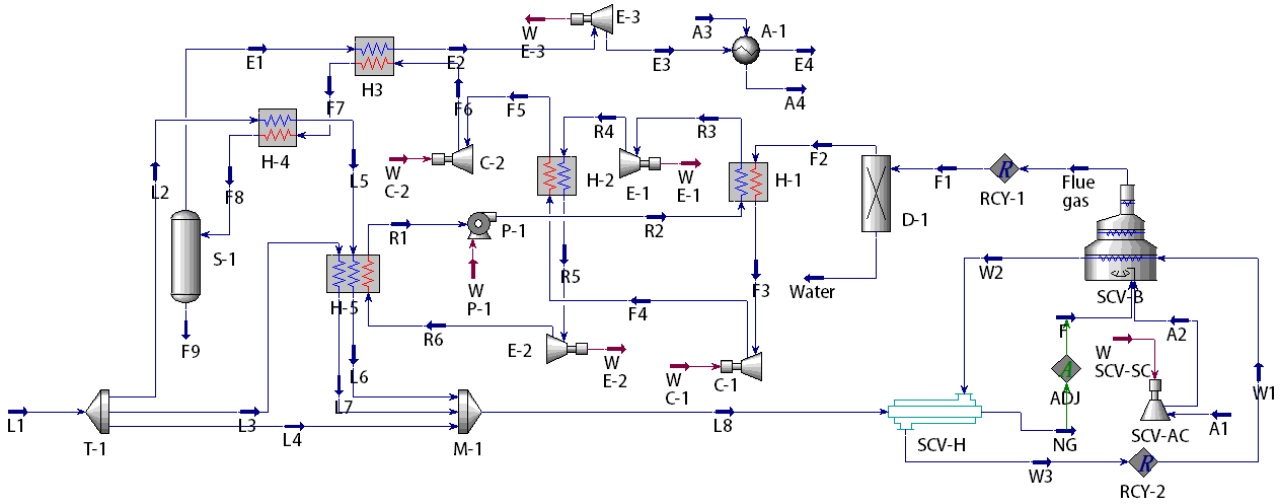

Figure 1. System A: HYSYS simulation model of SCV flue gas carbon capture using LNG cold energy. D-1: flue gas dehydrator; H-1–H-5: heat exchanger; C-1–C-2: compressor; E-1–E-3: turbine; P-1: working fluid pump; M-1: mixer; A-1: air temperature heater; S-1: separator; T-1: tee; SCV-AC: SCV air compressor; SCV-H: SCV heat exchange coil; SCV-B: SCV burner.

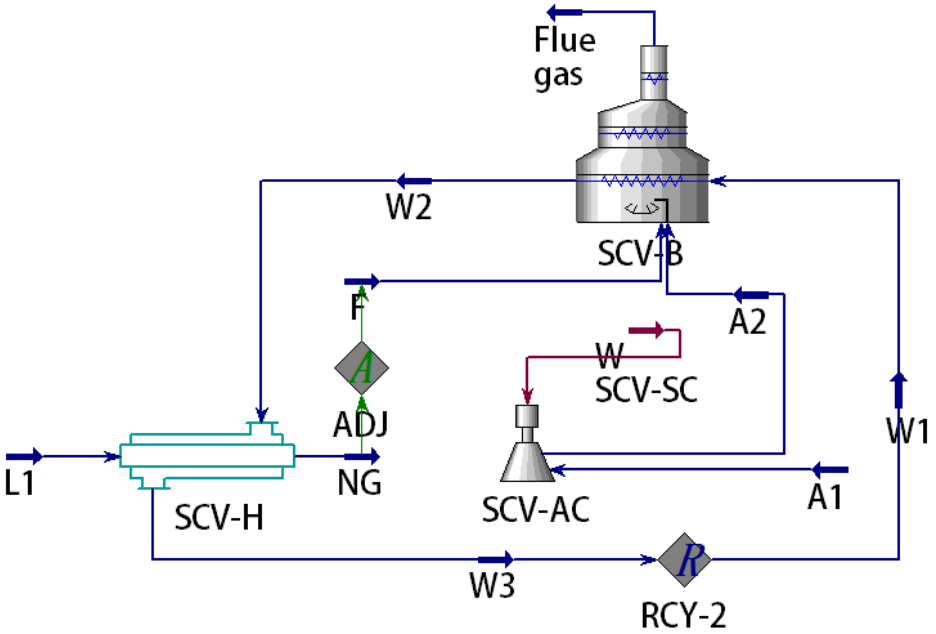

Figure 2. System B: HYSYS simulation model of conventional LNG regasification.

The SCV flue gas CC subsystem consists of a dehydrator, two compressors, four heat exchangers, and a separator. SCV flue gas goes through dehydration, cooling, compression, cooling, compression, precooling, condensation, and separation to achieve SCV flue gas CC. The process takes place through F1–F9, and F9 contains high CO_2 concentration. The ORC subsystem is composed of a working fluid pump, two turbines, and three heat exchangers. The working fluid, composed of methane and ethane, successively goes through the cyclic process of condensation liquefaction, pressurization, evaporation, expansion, reheat, secondary expansion, and condensation liquefaction, which is the R1–R6 route. The exhausted gas DEC subsystem consists of a heat exchanger, an air temperature heater, and a turbine, and the process is takes place through E1–E4. The LNG regasification subsystem consists of a tee, a mixer, and an SCV that consists of the heat exchanger, burner, and air compressor, and the LNG process takes place through L1–L8. In System A and System B, A1–A4 is air, W1–A3 is softening water, F is fuel gas, and the isentropic efficiency of the turbine, pump, and compressor is 0.85.

3. Mathematical Model and Method of Analysis

3.1. Assumptions

To simplify the model of the system, the following assumptions are made.

(1). The system is running stably;
(2). LNG and fuel gas composition consist of methane, ethane, propane, and nitrogen. The molar concentrations are 90.38%, 5.37%, 4.04%, and 0.21% respectively;
(3). Air is an ideal gas composed of 21% oxygen and 79% nitrogen;
(4). The working fluid is composed of methane and ethane. The molar concentrations are 20%, and 80%, respectively;
(5). The pressure drop of heat exchangers and pipelines and the heat transfer between the system and the environment are ignored.

3.2. Thermodynamic Model

The first law of thermodynamics equation of the equipment of System A is shown in Table 1.

Table 1. The first law of thermodynamics Equation of System A equipment.

Equipment	The First Law of Thermodynamics Equation	Equipment	The First Law of Thermodynamics Equation
P-1	$W_{P-1} = m_{R1}(h_{R2} - h_{R1})$	H-1	$m_{R1}(h_{R3} - h_{R2}) = m_{F1}(h_{F2} - h_{F3})$
C-1	$W_{c-1} = m_{F3}(h_{F4} - h_{F3})$	H-2	$m_{R1}(h_{R5} - h_{R4}) = m_{F1}(h_{F4} - h_{F5})$
C-2	$W_{c-2} = m_{F5}(h_{F6} - h_{F5})$	H-3	$m_{F1}(h_{F7} - h_{F6}) = m_{E1}(h_{E1} - h_{E2})$
SCV-AC	$W_{scv-ac} = m_{A1}(h_{A2} - h_{A1})$	H-4	$m_{F1}(h_{F8} - h_{F7}) = m_{L2}(h_{L2} - h_{L5})$
E-1	$W_{E-1} = m_{R4}(h_{R3} - h_{R4})$	T-1	$m_{L1}h_{L1} = m_{L2}h_{L2} + m_{L3}h_{L3} + m_{L4}h_{L4}$
E-2	$W_{E-2} = m_{R6}(h_{R5} - h_{R6})$	M-1	$m_{L6}h_{L6} + m_{L7}h_{L7} + m_{L4}h_{L4} = m_{L8}h_{L8}$
E-3	$W_{E-3} = m_{E1}(h_{E2} - h_{E3})$	D-1	$m_{F8}h_{F8} = m_{F9}h_{F9} + m_{E1}h_{E1}$
SCV-B	$m_{W1}(h_{W1} - h_{W2}) + m_{A1}h_{A2} + W_F = m_F h_F$	S-1	$m_{F1}h_{F1} = m_{F2}h_{F2} + m_{Water}h_{Water}$
SCV-H	$m_{E1}(h_{E4} - h_{E3}) = m_{A3}(h_{A3} - h_{A4})$	A-1	$m_{L8}(h_{NG} - h_{L8}) = m_{W2}(h_{W2} - h_{W3})$
H-5	$m_{R1}(h_{R1} - h_{R6}) = m_{L2}(h_{L5} - h_{L6}) + m_{L3}(h_{L3} - h_{L7})$		

Exergy is defined as the maximum useful work that can be derived from the system when it reversibly reaches equilibrium with the reference environment. The physical exergy of each node in the process is defined as Equation (1). The exergy balance equation and exergy efficiency of the key equipment in System A are shown in Table 2.

$$E_i = m_i[(h_i - h_0) - T_0(s_i - s_0)] \quad (1)$$

where h_0 is reference enthalpy, kJ/kg; h is specific entropy, kJ/kg.; s is specific entropy, kJ/(kg·K); s_0 is reference entropy, kJ/(kg·K); and T_0 is reference temperature, K.

Table 2. The relationship between exergy balance and exergy efficiency of System A key equipment.

Equipment	Exergy Balance	Exergy Efficiency
P-1	$W_{P-1} + E_{R1} = E_{R2} + E_{D,P-1}$	$\eta_{P-1} = (E_{R2} - E_{R1})/W_{P-1}$
C-1	$W_{C-1} + E_{F3} = E_{F4} + E_{D,C-1}$	$\eta_{C-1} = (E_{F4} - E_{F3})/W_{C-1}$
C-2	$W_{C-2} + E_{F5} = E_{F6} + E_{D,C-2}$	$\eta_{C-2} = (E_{F6} - E_{F5})/W_{C-2}$
E-1	$E_{R3} = E_{R4} + W_{E-1} + E_{D,E-1}$	$\eta_{E-1} = W_{E-1}/(E_{R3} - E_{R4})$
E-2	$E_{R5} = E_{R6} + W_{E-2} + E_{D,E-2}$	$\eta_{E-2} = W_{E-2}/(E_{R5} - E_{R6})$
E-3	$E_{E2} = E_{E3} + W_{E-3} + E_{D,E-3}$	$\eta_{E-3} = W_{E-3}/(E_{E3} - E_{E4})$
H-1	$E_{R2} + E_{F2} = E_{D,H-1} + E_{F3} + E_{R3}$	$\eta_{H-1} = (E_{F3} - E_{F2})/(E_{R2} - E_{R3})$
H-2	$E_{R4} + E_{F4} = E_{R5} + E_{F5} + E_{D,H-2}$	$\eta_{H-2} = (E_{F5} - E_{F4})/(E_{R4} - E_{R5})$
H-3	$E_{E1} + E_{F6} = E_{E2} + E_{F7} + E_{D,H-3}$	$\eta_{H-3} = (E_{F7} - E_{F6})/(E_{E1} - E_{E2})$
H-4	$E_{L2} + E_{F7} = E_{L5} + E_{F8} + E_{D,H-4}$	$\eta_{H-4} = (E_{F8} - E_{F7})/(E_{L2} - E_{L5})$
H-5	$E_{L5} + E_{L3} + E_{R6} = E_{L6} + E_{L7} + E_{R1} + E_{D,H-5}$	$\eta_{H-5} = (E_{R1} - E_{R6})/(E_{L5} - E_{L6} + E_{L3} - E_{L7})$

3.3. Method of Analysis

The thermodynamic analysis is based on the first and second laws of thermodynamics. The subscripts of the following equations correspond to the state points in Figures 2 and 3. The energy consumption of System A and System B is defined by Equations (2) and (3), respectively.

$$W_A = W_E + W_F \tag{2}$$

$$W_B = W_{SCV-AC} + W_F \tag{3}$$

$$W_E = W_{SCV-AC} + W_{CC} - W_{ORC} - W_{DEC} \tag{4}$$

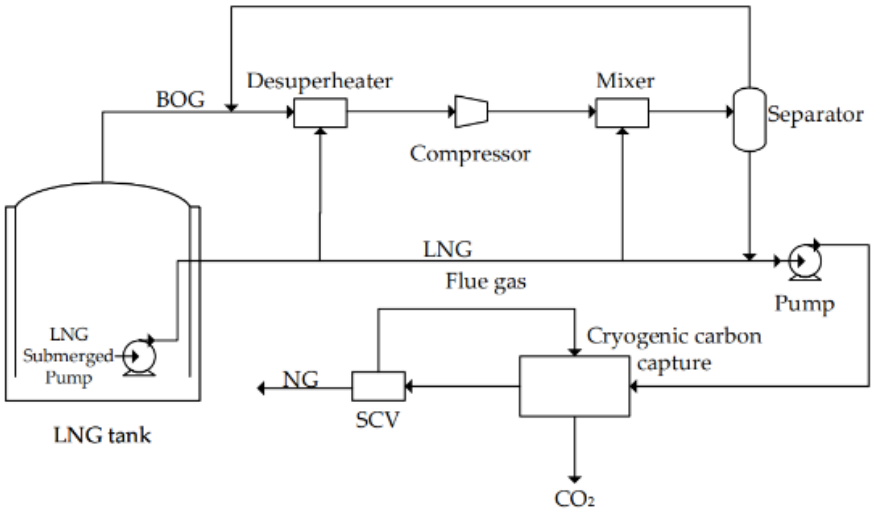

Figure 3. Low carbon operation strategy of the LNG receiving terminal.

The net power of the ORC subsystem and the exhausted gas DEC subsystem are defined by Equations (5) and (6), respectively.

$$W_{ORC} = m_{R1}[(h_{R3} - h_{R4}) + (h_{R5} - h_{R6}) - (h_{R2} - h_{R1})] \tag{5}$$

$$W_{DEC} = m_{E1}(h_{E2} - h_{E3}) \tag{6}$$

The energy consumption of the flue gas CC subsystem, SCV air compressor, and fuel gas consumed by SCV are defined by Equations (7)–(9), respectively.

$$W_{CC} = m_{F1}[(h_{F4} - h_{F3}) + (h_{F6} - h_{F5})] \tag{7}$$

$$W_{SCV-AC} = m_{A1}(m_{A2} - m_{A1}) \tag{8}$$

$$W_F = m_F q_F \tag{9}$$

Among them: W is power, kW; m is mass flow rate, kg/s; h is specific enthalpy, kJ/kg; and q is high calorific value, kJ/kg.

The exergy efficiency of System A (without LNG regasification subsystem) and the utilization rate of LNG cold exergy are defined by Equations (10) and (11), respectively.

$$\eta_E = \frac{E_{F9} - E_{F2}}{E_{L2} + E_{L3} - E_{L6} - E_{L7} + W_E} \tag{10}$$

$$\eta_{E-LNG} = \frac{E_{R1} - E_{R6} + E_{F8} - E_{F7}}{E_{L2} + E_{L3} - E_{L6} - E_{L7}} \tag{11}$$

The carbon emissions of System A and System B can be divided into direct carbon emissions caused by flue gas and indirect carbon emissions caused by electricity consumption. The Emission-Factor Approach is used for indirect carbon emissions calculation, and the Experiment Approach is used for direct carbon emissions [27]. The carbon emissions of System A and System B are defined by Equations (12) and (13), respectively.

$$P_A = W_E \times EF + C_{E4} \tag{12}$$

$$P_B = W_{SCV-AC} \times EF + C_{Fluegas} \tag{13}$$

The CO_2 capture rate of the system is Equation (14).

$$\eta_{CC} = \frac{C_{F9}}{C_{F2}} \times 100 \tag{14}$$

where EF is the power supply emission factor, 0.8885 kg/(kW. h), and C is the mass flow rate of CO_2 in logistics, kg/h.

4. Results and Discussion

In this paper, HYSYS software was used to simulate the SCV flue gas carbon capture process using LNG cold energy, and the P–R equation was used to calculate the thermodynamic properties of each logistics. In this section, the thermodynamic performance of System A was studied based on the first and second laws of thermodynamics, and the energy consumption and carbon emissions of System A and System B are comparatively analyzed. In addition, the sensitivity analysis of key parameters to the performance of System A was studied. Finally, the parameters were optimized using Aspen HYSYS software. Initial data of the process simulation for System A and System B are listed in Table 3.

Table 3. Initial simulation conditions for System A and System B.

Condition	Value	Condition	Value
Environment temperature (K)	274.15	SCV-AC outlet pressure (kPa)	116.5
Environment pressure (kPa)	101.325	R1 Composition	Methane:Ethane = 2:8
Heat exchanger pinch temperature (K)	3.5 [28]	P-1 inlet temperature (K)	138.15
Pump adiabatic efficiency (%)	85	P-1 inlet pressure (kPa)	150
Compressor and turbine adiabatic efficiency (%)	85	P-1 outlet pressure (kPa)	1300
L1 Mass flow rate (t/h)	196.1	E-1 outlet pressure (kPa)	460
L1 Temperature (K)	120.85	Carbon capture temperature (K)	143.15 [20]
L1 Pressure (kPa)	9101	Carbon capture pressure (kPa)	930
NG Temperature (K)	297.15	C-1 outlet pressure (kPa)	310
F Temperature (K)	288.15	E-3 outlet pressure (kPa)	101.325
F Pressure (kPa)	601	E4 Temperature (K)	269.15

The simulation results of flue gas and exhausted gas in System A and System B are shown in Table 4, and the simulation results of LNG and the working fluid in System A are shown in Table 5. According to Table 4, solid CO_2 will appear at state points F7, F8, and F9. This is due to the low concentration of CO_2 in the flue gas, resulting in the freeze point temperature of the flue gas being greater than the dew point temperature [29]. Therefore, in the process of cooling the flue gas, the freezing point of the flue gas will first be reached, and solid phase CO_2 will be formed, which may lead to blockage of the heat exchanger. To solve the problem of blockage, dynamically operated packed beds [30] and condensate separators [29] can be used to replace heat exchangers in the actual project. The hybrid membrane cryogenic process [25,26] can also be used to increase the concentration of CO_2 in the flue gas, so that the dew point temperature of the flue gas is greater than the freezing point, so as to prevent the formation of solid CO_2.

Table 4. Simulation results of flue gas and exhausted gas in System A and System B.

Node	*T* (K)	*P* (kPa)	*m* (kg/h)	Vapor Fraction	Freeze Point (K)	Composition (mol%)			
						H_2O	N_2	O_2	CO_2
Flue gas (B)	306.17	116.5	62,947.9	0.892	170.79	14.71	69.58	8.10	7.61
Flue gas (A)	306.17	116.5	58,449.4	0.892	170.79	14.71	69.58	8.10	7.61
F2	306.17	116.5	52,932	1	171.21	0	81.58	9.50	8.92
F3	174.06	116.5	52,932	1	171.21	0	81.58	9.50	8.92
F4	239.94	310.0	52,932	1	180.33	0	81.58	9.50	8.92
F5	231.84	310.0	52,932	1	180.33	0	81.58	9.50	8.92
F6	329.93	930.0	52,932	1	191.30	0	81.58	9.50	8.92
F7	176.75	930.0	52,932	0.980	191.30	0	81.58	9.50	8.92
F8	143.15	930.0	52,932	0.913	191.30	0	81.58	9.50	8.92
F9	143.15	930.0	6748.2	0	215.91	0	1.52	0.38	98.10
E1	143.15	930.0	46,183.8	1	137.29	0	89.20	10.37	0.43
E2	326.43	930.0	46,183.8	1	137.29	0	89.20	10.37	0.43
E3	195.03	101.3	46,183.8	1	128.78	0	89.20	10.37	0.43

Table 5. Simulation results of LNG and working fluid in System A.

Node	*T* (K)	*P* (kPa)	*m* (kg/h)	Node	*T* (K)	*P* (kPa)	*m* (kg/h)
R1	138.15	150.0	10,452.9	L2	120.85	9101	23,962.1
R2	139.47	1300.0	10,452.9	L3	120.85	9101	40,000.0
R3	257.26	1300.0	10,452.9	L4	120.85	9101	132,137.9
R4	212.21	460.0	10,452.9	L5	173.25	9101	23,962.1
R5	136.45	460.0	10,452.9	L6	185.31	9101	23,962.1
R6	194.15	150.0	10,452.9	L7	160.65	9101	40,000.0
L1	120.85	9101	196,100.0	L8	137.05	9101	196,100.0

4.1. Analysis of System Carbon Emission and Energy Consumption

Equations (2)–(9) and Equations (12)–(14) were used to calculate the energy consumption and carbon emissions of System A and System B, respectively. The calculation results are shown in Table 6. When the LNG cold energy was used for SCV flue gas carbon capture, the fuel gas consumption, energy consumption, and carbon emissions of the system were reduced by 7.16%, 6.3%, and 89.6%, respectively. The CO_2 capture rate and CO_2 capture capacity of System A were 95.6% and 6663.5 kg/h, respectively, and the direct carbon emissions generated during SCV operation were significantly reduced.

Table 6. Energy consumption and carbon emissions of the system.

System	A	B
Direct carbon emissions (kg/h)	304.4	7504.2
Fuel gas consumption (kg/h)	2520.4	2714.7
Electricity consumption of the system (kW)	561.5	220.4
W_{SCV-AC} (kW)	204.6	220.4
W_{ORC} (kW)	316.4	~
W_{DEC} (kW)	1691.3	~
W_{CC} (kW)	2364.6	~
Energy consumption of the system (kW)	38,514.8	41,100.2
Carbon emissions of the system (kg/h)	803.3	7700.0
Carbon capture rate (%)	95.6	~

Therefore, utilizing LNG cold energy to capture the carbon of SCV flue gas can provide a feasible scheme for the low-carbon operation of the LNG receiving terminal, as shown in Figure 3. After the LNG from the tank is pressurized, it first enters the CCC unit to release cold energy and then enters the SCV gasification unit. The flue gas generated by the SCV operation enters the CCC unit for carbon capture, which ultimately reduces the direct carbon emissions of the LNG receiving terminal.

4.2. Exergy Analysis

The reference states for exergy calculations were set as 274.15 K and 101.325 kPa. The calculation results of exergy input, output, and loss of System A (without LNG regasification subsystem) under the initial conditions are shown in Table 7. It can be seen that the exergy input contained the physical exergy of the flue gas and LNG, as well as the electric power input through compressors and pumps. The exergy output included the physical exergy of CO_2 and the mechanical work produced by the ORC subsystem and the DEC subsystem. As calculated by Equations (10) and (11), the exergy efficiency and LNG cold exergy utilization rate of System A (excluding the LNG regasification subsystem) were 13.32% and 77.61%, respectively. When compared with the literature [21,22], the exergy efficiency of the system is low.

Table 7. The calculation results of exergy input, output, and loss in System A.

Project	Term	Value (kW)
Input	LNG (L1, L2)	17,165.4
	Fuel gas (F2)	173.2
	C-1	937.3
	C-2	1427.3
	P-1	6.8
Output	LNG (L6, L7)	14,447.1
	F9	625.7
	E-1	157.8
	E-2	165.4
	E-3	1691.3
Loss	E3	306.2
	Equipment of the system	2316.5
Exergy efficiency (%)		13.32
The utilization rate of LNG cold exergy (%)		77.61

The exergy loss percentages of the System A components are shown in Figure 4, including heat exchangers, pumps, compressors, and turbines. Because of the temperature difference in the heat transfer process, the main exergy losses within the heat exchangers were the main exergy losses of the system (more than 72.4%). The exergy loss of other equipment accounted for 27.6% of system exergy loss, and the exergy loss of E-3 even reached

14.6%. For analyzing the exergy losses in heat exchangers, the temperature differences under the initial conditions in heat exchangers were calculated as shown in Figure 5. The LMTD (log mean temperature difference) of H-1, H-3, H-4, and H-5 was 12.21 K, 10.76 K, 12.32 K, and 20.41 K, respectively. In the heat exchanger (H-1, H-4, H-5), the matching degree of the temperature–heat flow curve of the cold and hot logistics was not high, resulting in a higher LMTD of the heat exchanger, which increased the exergy loss of the heat exchanger and reduced the exergy efficiency of the system.

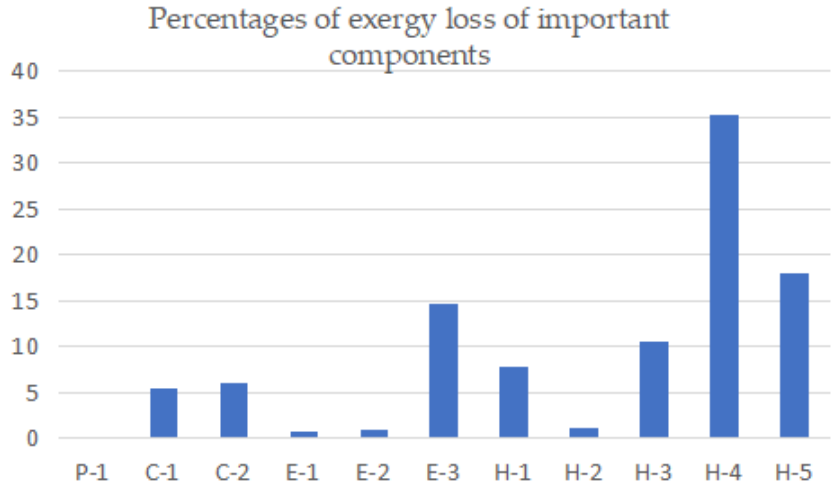

Figure 4. The exergy loss percentage of important components in System A.

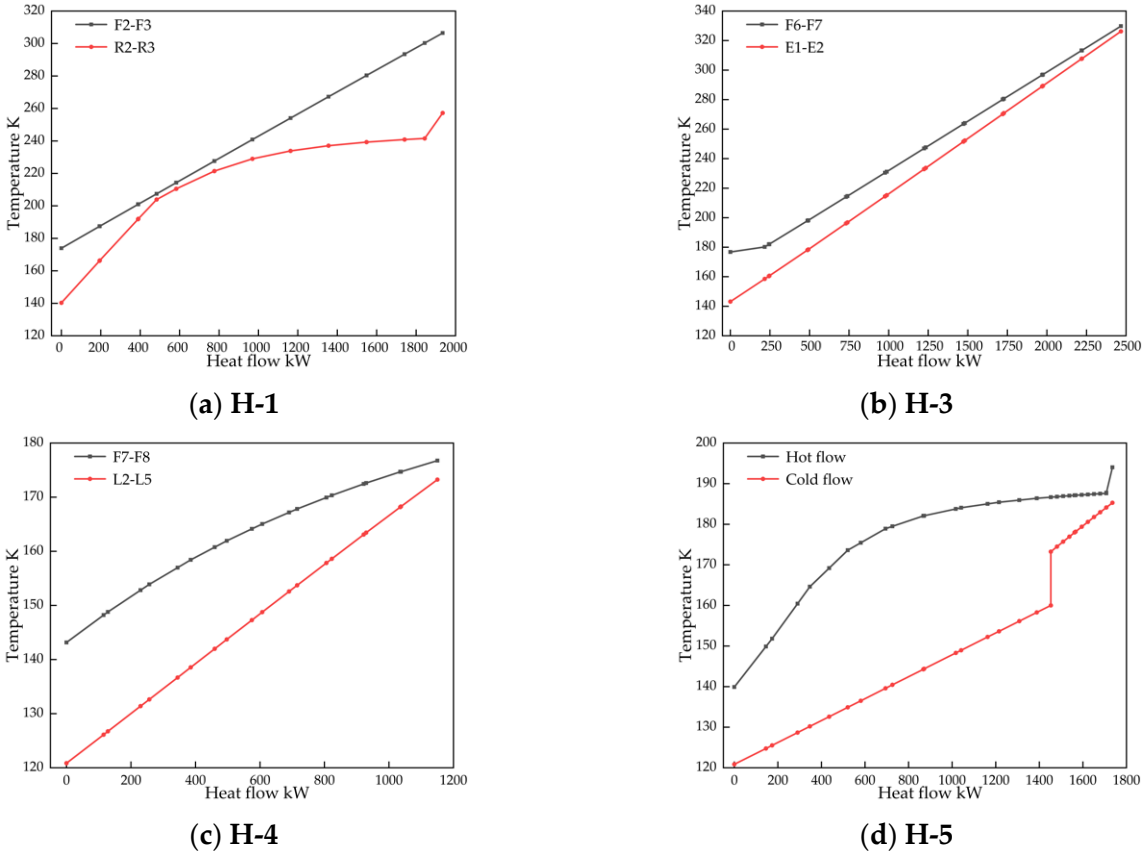

Figure 5. The temperature difference and heat flow in heat exchangers.

4.3. Sensitivity Analysis of Key Parameters on the System Performance

4.3.1. Working Fluid Evaporation Pressure

The evaporation pressure of the working fluid will affect the net work and efficiency of the ORC. The effect of the working fluid evaporation pressure on system performance is shown in Figure 6. The electricity consumption and energy consumption of the system increased with the increment of the evaporation pressure of the ORC working fluid. According to the P–H phase diagram (Figure 7) of the working fluid, with the increase in the ORC working fluid evaporation pressure, the cold energy required for the condensing working fluid in the H-5 heat exchanger decreased, and the cold energy released in the heat exchanger H-1 and H-2 decreased at the same time. This then led to a decrease in the SCV inlet LNG temperature and an increase in compressor inlet temperature for compressors C-1 and C-2, which increased SCV fuel gas consumption, power consumption, and system energy consumption. As the evaporation pressure of the working fluid increased, the direct carbon emission of the system increases slightly, which coupled with the growth of the electricity consumption of the system, so the carbon emission of the system also increased.

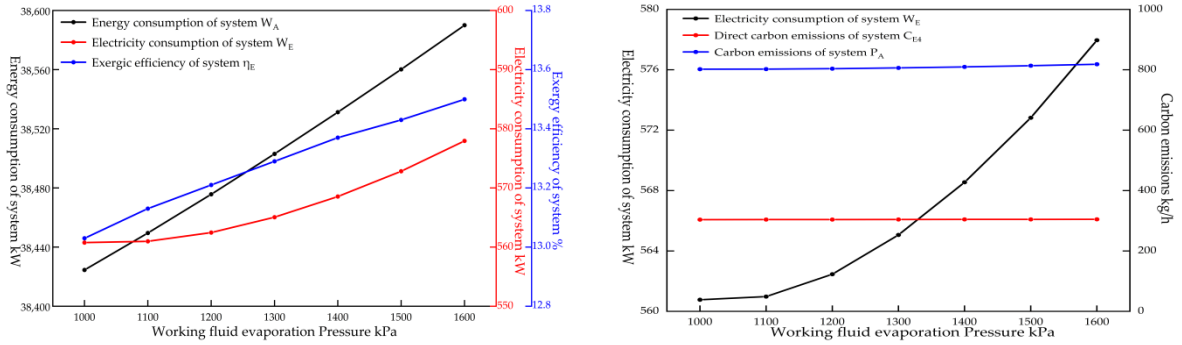

Figure 6. The effect of evaporation pressure of working fluid on system performance. (**a**): System energy consumption and exergy efficiency; (**b**): System electricity consumption and carbon emissions.

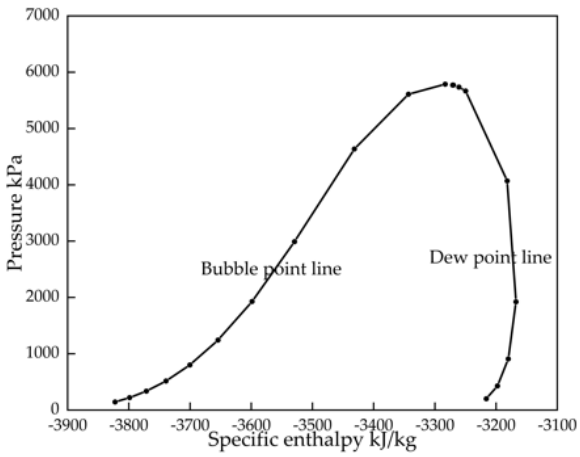

Figure 7. P-H phase diagram of the working fluid.

4.3.2. CO_2 Capture Pressure

The CO_2 capture pressure affects the SCV flue gas CC amount, the system energy consumption, and the system exergy efficiency. The effect of CO_2 capture pressure on system performance is shown in Figure 8. The energy consumption and electricity consumption of the system increased as the CO_2 capture pressure increased. With the increase in CO_2 capture pressure, the energy consumption of compressors C-1 and C-2 increased sharply, and the heat energy carried by the compressor outlet increased, resulting in a higher ORC working fluid flow, an augment in the cold energy needed by the heat exchanger H-5,

and the LNG temperature rise at the SCV inlet. This resulted in a small reduction in SCV fuel gas consumption, a substantial increase in system electricity consumption, and an increase in system energy consumption. With the increase in CO_2 capture pressure, the irreversibility of compressor C-1, compressor C-2, and turbine E-3 enhanced. The system exergy loss increased while the system exergy efficiency decreased. Besides, the carbon capture amount of the system increased, and the direct carbon emissions of the system were reduced. As the electricity consumption of the system increased, the carbon emission of the system first decreased and then increased. When the CO_2 capture pressure was 530 kPa, the system had the lowest carbon emissions.

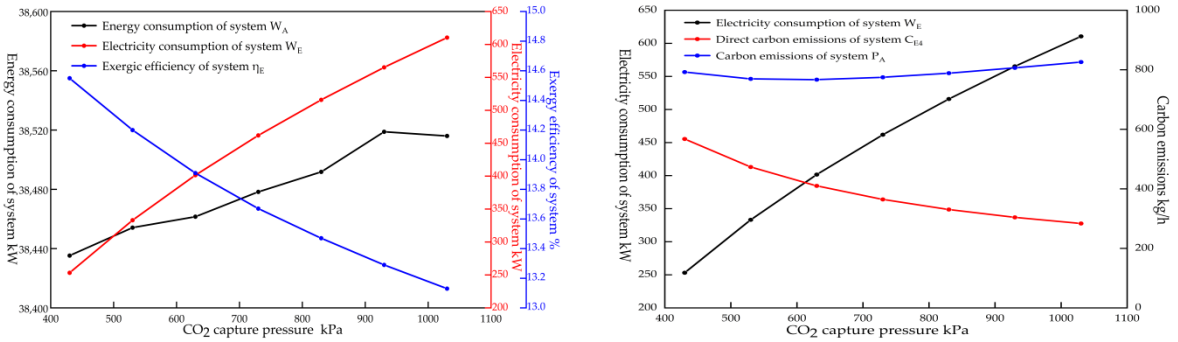

(**a**) (**b**)

Figure 8. The effect of CO_2 capture pressure on system performance. (**a**): System energy consumption and exergy efficiency; (**b**): System electricity consumption and carbon emissions.

4.3.3. CO_2 Capture Temperature

The CO_2 capture temperature influences the SCV flue gas CC amount, the system energy consumption, and the system exergy efficiency, and the effects on the system performance are shown in Figure 9. The system energy consumption increased, the electricity consumption and exergy efficiency of the system decreased, and the CC amount of the system greatly reduced as the CO_2 capture temperature increased, so the direct carbon emission of the system increased significantly. Even when the electricity consumption of the system was reduced, the carbon emissions of the system still increased significantly. The CO_2 capture temperature increased, the cold energy needed by the heat exchanger H-3 decreased, and the LNG temperature at the SCV inlet decreased, thus increasing SCV fuel gas consumption. In addition, the inlet temperature of turbine E-3 increased, and its net work increased. Equation (10) can explain that the decrease in system exergy efficiency was due to the reduction in the CC amount of the system.

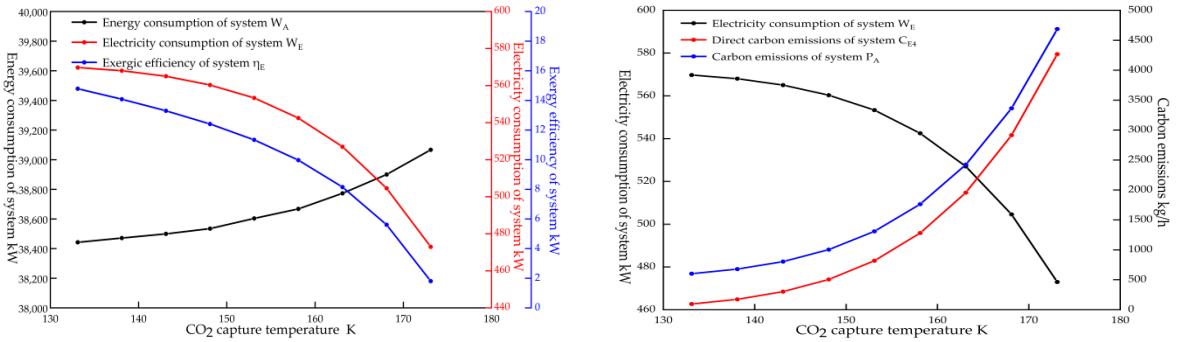

(**a**) (**b**)

Figure 9. The effect of CO_2 capture temperature on system performance. (**a**): System energy consumption and exergy efficiency; (**b**): System electricity consumption and carbon emissions.

4.4. Key Parameter Optimization

Through the sensitivity analysis of the above important process parameters, it was found that the evaporation pressure of the working fluid was sensitive to the system energy consumption and less sensitive to the system direct carbon emission, while the CO_2 capture pressure and CO_2 capture temperature were sensitive to the system energy consumption and the direct carbon emissions. HYSYS software was used to optimize the key parameters of the system to achieve the lowest operating cost of the system, and the optimization variables were the evaporation pressure of the working fluid P_{R2}, CO_2 capture pressure P_{F6}, and CO_2 capture temperature T_{F8}. The objective function is shown in Equation (15).

$$\min F(P_{R2}, P_{F6}, T_{F8}) = 3600am_F + bW_E + dC_{E4} \quad (15)$$

where, a is fuel gas price, 8.3 ¥/kg; b is electricity price, 0.62 ¥/(kW·h); and d is carbon trading price, 0.07 ¥/kg.

The constraint conditions are Equations (16)–(18).

$$1000 \leq P_{R2} \leq 1600 \quad (16)$$

$$430 \leq P_{F6} \leq 1030 \quad (17)$$

$$133.15 \leq T_{F8} \leq 173.15 \quad (18)$$

The optimization results were P_{R2} = 1300 kPa, P_{F6} = 750 kPa, and T_{F8} = 143.15 K. After optimization, the fuel gas consumption of the system was 2524 kg/h, the electric energy consumption of the system was 473.1 kW, the CO_2 capture capacity of the system was 6620.4 kg/h, the carbon capture rate of the system was 94.9%, the carbon emissions of the system were 777.4 kg/h, the exergy efficiency of the system was 13.63%, and the utilization rate of the LNG cold exergy was 77.49%.

5. Conclusions

The SCV flue gas carbon capture system based on LNG cold energy has been proposed, and the thermodynamic and carbon emissions analyses of this system were conducted. HYSYS software was used to optimize the system process parameters to seek the optimal design process. The main conclusions drawn from the present work are summarized as follows:

- Under the steady-state conditions, the energy consumption and carbon emissions of a SCV flue gas carbon capture system based on LNG cold energy were 38,514.8 kW and 803.3 kg/h, respectively. The CO_2 capture rate was 95.6%, the CO_2 capture capacity was 6663.5 kg/h, and the exergy efficiency was 13.32%.
- The SCV flue gas carbon capture system based on LNG cold energy utilized most of the LNG physical exergies. The utilization rate of LNG cold exergy was 77.61%, and the equipment with high exergy destructions was the heat exchanger.
- In order to improve the system's exergy efficiency and reduce the energy consumption and carbon emissions of the system, the working fluid evaporation pressure, CO_2 capture pressure, and CO_2 capture temperature should be appropriately reduced within a certain range.
- Under the final optimal conditions, the system was able to reach an exergy efficiency of 13.63%, an LNG cold exergy utilization rate of 77.49%, and a CO_2 capture rate of 94.9%.
- Compared to the conventional LNG regasification system (System B), the SCV flue gas carbon capture system based on LNG cold energy proposed in this paper has the characteristics of low energy consumption and low carbon emission. Subsequent process improvements can be combined with membrane separation technology.

Author Contributions: Conceptualization, K.H. and K.C.; methodology, K.H.; software, K.C.; formal analysis, K.C.; investigation, K.H.; resources, L.W.; data curation, L.W.; writing—original draft preparation, K.C. and C.H.; writing—review and editing, C.H.; visualization, J.C. All authors have read and agreed to the published version of the manuscript.

Funding: This research received no external funding.

Data Availability Statement: Not applicable.

Conflicts of Interest: The authors declare no conflict of interest.

References

1. Chen, R.; Zhang, X.Y. Characteristics and challenges of global carbon neutrality LNG trading. *Pet. New Energy* **2021**, *33*, 39–42.
2. Zhang, W.D.; Jin, Y.S.; Fu, P.H.; Li, X.H. Calculation and analysis of greenhouse gas emission of LNG terminals. *Petrochem. Saf. Environ. Prot. Technol.* **2018**, *34*, 49–53.
3. Ma, G.G.; Wu, X.N.; Wang, Y.C. *Liquefied Natural Gas Technology*; Petroleum Industry Press: Beijing, China, 2012.
4. Honzawa, T.; Kai, R.; Seino, M.; Nishiie, T.; Suzuki, Y.; Okada, A.; Wazaki, K.; Kurose, R. Numerical and experimental investigations on turbulent combustion fields generated by large-scale submerged combustion vaporizer burners with water spray equipment. *J. Nat. Gas Sci. Eng.* **2020**, *79*, 103158. [CrossRef]
5. Li, W.; Wang, Y.C. The development trend and impact of global carbon-neutral LNG trade. *Int. Pet. Econ.* **2022**, *30*, 72–79.
6. Bu, X.P. CO_2 capture technologies and application. *Clean Coal Technol.* **2014**, *5*, 19.
7. Song, C.; Liu, Q.; Deng, S.; Li, H.; Kitamura, Y. Cryogenic-based CO_2 capture technologies: State-of-the-art developments and current challenges. *Renew. Sustain. Energy Rev.* **2019**, *101*, 265–278. [CrossRef]
8. He, T.B.; Chong, Z.R.; Zheng, J.J.; Ju, Y.L.; Linga, P. LNG cold energy utilization: Prospects and challenges. *Energy* **2019**, *170*, 557–568. [CrossRef]
9. Kanbur, B.B.; Xiang, L.M.; Dubey, S.; Choo, F.H.; Duan, F. Cold utilization systems of LNG: A review. *Renew. Sustain. Energy Rev.* **2017**, *79*, 1171–1188. [CrossRef]
10. Shi, H.Q. An Integration Process of ORC and CO_2 Recovery Bases on LNG Cold Energy Utilization. Master's Thesis, Northeastern University, Shengyang, China, 2015.
11. Huang, M.B.; Lin, W.S.; He, H.M.; Gu, A.Z. LNG cold energy utilized in a transcritical CO_2 rankine cycle and CO_2 Recovery by liquefaction. *Cryog. Supercond.* **2009**, *4*, 17–21.
12. Wang, D.G. Analysis of the power cycle technologies for CO_2 liquefaction with LNG coldness energy. *Shandong Chem. Ind.* **2014**, *9*, 105.
13. Xiong, Y.Q.; Hua, B. Integration of energy power system in CO_2 capture by utilization of cold energy from liquefied natural gas. *CIESC J.* **2010**, *12*, 3142–3148.
14. Ghorbani, B.; Mehrpooya, M.; Rooholamini, S. Novel integrated structure of carbon dioxide liquefaction energy storage system using solar energy. *J. Energy Storage* **2020**, *31*, 101641. [CrossRef]
15. Liu, Y.; Han, J.T.; You, H.L. Performance analysis of a CCHP system based on SOFC/GT/CO_2 cycle and ORC with LNG cold energy utilization. *Int. J. Hydrogen Energy* **2019**, *44*, 29700–29710. [CrossRef]
16. Yu, H.S.; Gundersen, T.; Gençer, E. Optimal liquified natural gas (LNG) cold energy utilization in an Allam cycle power plant with carbon capture and storage. *Energy Convers. Manag.* **2021**, *228*, 113725. [CrossRef]
17. Liang, W.X.; Yu, Z.T.; Bai, S.Z.; Li, G.X.; Wang, D.H. Study on a near-zero emission SOFC-based multi-generation system combined with organic Rankine cycle and transcritical CO_2 cycle for LNG cold energy recovery. *Energy Convers. Manag.* **2022**, *253*, 115188. [CrossRef]
18. Ouyang, T.C.; Tian, J.Q.; Wu, W.C.; Xie, S.T.; Li, D.F. Energy, exergy and economic benefits deriving from LNG-fired power plant: Cold energy power generation combined with carbon dioxide capture. *Renew. Energy* **2022**, *195*, 214–229. [CrossRef]
19. Xu, J.X.; Lin, W.S. A CO_2 cryogenic capture system for flue gas of an LNG-fired power plant. *Int. J. Hydrogen Energy* **2017**, *42*, 18674–18680. [CrossRef]
20. Rifka, T.; Morosuk, T.; Tsatsaronis, G. Carbon capture and storage using low-temperature post-combustion technologies. *Energy Sources Part A* **2019**, *43*, 3371–3380. [CrossRef]
21. Liu, Y.; Han, J.T.; You, H.L. Exergoeconomic analysis and multi-objective optimization of a CCHP system based on LNG cold energy utilization and flue gas waste heat recovery with CO_2 capture. *Energy* **2020**, *190*, 116201. [CrossRef]
22. Zhao, L.; Dong, H.; Tang, J.J.; Cai, J.J. Cold energy utilization of liquefied natural gas for capturing carbon dioxide in the flue gas from the magnesite processing industry. *Energy* **2016**, *105*, 45–56. [CrossRef]
23. Bao, J.J.; Zhang, L.; Song, C.X.; Zhang, N.; Guo, M.G.; Zhang, X.P. Reduction of efficiency penalty for a natural gas combined cycle power plant with post-combustion CO_2 capture: Integration of liquid natural gas cold energy. *Energy Conv. Manag.* **2019**, *198*, 111852. [CrossRef]
24. Pan, Z.; Wu, J.J.; Chen, Y.N.; Zhao, S.Y. Simulation and performance optimization of a poly-generation system based on LNG cold energy utilization. *Oil Gas Storage Transp.* **2022**, *41*, 810–818.

25. Belaissaoui, B.; Le Moullec, Y.; Willson, D.; Favre, E. Hybrid membrane cryogenic process for post-combustion CO_2 capture. *J. Membr. Sci.* **2012**, *415*, 424–434. [CrossRef]
26. Li, R.; Lian, S.H.; Zhang, Z.Z.; Song, C.F.; Han, R.; Liu, Q.L. Techno-economic evaluation of a novel membrane-cryogenic hybrid process for carbon capture. *Appl. Therm. Eng.* **2022**, *200*, 117688. [CrossRef]
27. Liu, M.D.; Meng, J.J.; Liu, B.H. Progress in the studies of carbon emission estimation. *Trop. Geogr.* **2014**, *34*, 248–258.
28. Lu, Y.W.; Yang, H.C.; Lv, P.F.; Liu, G.L.; Ma, C.F.; Wu, Y.T. Parametric analysis and working fluid selection of power generation system based on LNG cold energy. *J. Beijing Polytech. Univ.* **2011**, *37*, 1874–1879.
29. Zhou, Y.Z. Performance Study on Carbon Capture Technology Based on Gas-Solid Phase Separation. Master's Thesis, Tianjin University, Tianjin, China, 2019.
30. Tuinier, M.J.; Annaland, M.V.; Kramer, G.J.; Kuipers, J.A.M. Cryogenic CO_2 capture using dynamically operated packed beds. *Chem. Eng. Sci.* **2010**, *65*, 114–119. [CrossRef]